Interaction of doping impurities with the 30° partial dislocations in SiC: An *ab initio* investigation

Fabio Bernardini* and Luciano Colombo

SLACS (INFM-CNR)and Department of Physics, University of Cagliari, Cittadella Universitaria, I-09124 Monserrato (CA), Italy

(Received 8 February 2005; revised manuscript received 21 June 2005; published 17 August 2005)

In this work we investigated, by means of state-of-the-art first principle techniques, the effect of impurity segregation on the energetics, the structure, and the electronic properties of dislocation cores. We find that for the species we considered, Al, P, B, and N, i.e., the most common dopants in SiC, the impurity-dislocation interaction is attractive and that segregation energies are comparable or larger than dislocations reconstruction energies. As to the doping properties of the impurities they are deactivated by the interaction with the dislocation core environment, with the noticeable exception of P. We rationalized our results in terms of the effect of the dopants on the dislocation core band structure.

DOI: 10.1103/PhysRevB.72.085215 PACS number(s): 61.72.Lk, 71.55.−i, 62.20.−x

I. INTRODUCTION

The increasing need for high temperature electronics in the aerospace, automotive and deep-well drilling industry has stimulated the interest for the fabrication of silicon carbide based devices. Indeed SiC-based electronics and sensors can operate in hot environments at temperatures up to 600 °C where conventional silicon-based electronics (limited to 350 °C) cannot work. The useful properties of SiC have been known for decades, but the fabrication of devices was hindered by the extreme low quality of the bulk material. This situation changed after the development of a new technique, namely the modified Lely seeded sublimation growth which allowed the fabrication of acceptably large and reproducible single-crystal SiC wafers of good electrical quality.[1,2] In spite of this progress, some crucial technical obstacles still remain to be solved before SiC can achieve its true potential. In particular it is of paramount importance to improve crystal growth and doping techniques. The most important extended defects with detrimental effects in SiC are micropipes and dislocations. They adversely affect the properties of junctions, causing leakage currents. It is therefore important to understand the structure and the electronic properties of those defects.

Dislocations in SiC can originate both as the result of imperfect crystal growth and as the outcome of material processing. Indeed the low solubility and the limited diffusivity of candidate dopants in SiC[3,4] makes ion implantation the method of choice for dopant incorporation. During the implantation process, the SiC lattice is damaged, and following post-implant high-temperature annealing dislocation loops are formed.[5] After implantation SiC samples are characterized by the coexistence of dislocations and dopants. The interaction among them is known to influence the mobility and electrical properties of dislocations and impurities. The study of the interaction between impurities and dislocations in semiconductors is both of technological and fundamental interest. It is known that impurities tend to segregate near the dislocation core hindering their motion.[6] Moreover impurities trapped at dislocation cores are often deactivated.

This kind of behavior has been recently investigated in silicon for selected dislocation geometries and dopants,[7–10] while for other semiconductors only few works are available in literature.[11,12] In this work we choose to focus our attention on the 3*C*-SiC (zinc-blend) phase of this material, since a direct comparison with the results obtained on other zinc-blende structure semiconductors is possible. A few calculations performed on the 4*H*-SiC (hexagonal) phase show that the structural and, for the most part, the electronic properties of the dislocations are not dependent on the structural details of the bulk system. Indeed the core atomic environment for the dislocations occurring in different SiC polytypes are identical up to third-nearest neighbors, suggesting that core structures of dislocations are very similar in all polytypes. In zinc-blende semiconductors the most common dislocations belong to the {111} glide set, lying along the ⟨110⟩ direction. It is energetically favorable for pure dislocations to dissociate into (30° and 90°) partial dislocations, forming staking fault between the partials. Both have been investigated by Blumenau *et al.*[13] in pure SiC. Here we include the investigation of the interaction of the 30°-partial dislocations with the most common impurities.

This paper is organized as follows. Section II describes the method used in our investigation. Section III presents the results of our calculations for cubic SiC, while a comprehensive discussion is deferred to Sec. IV. In Sec. V we extend our discussion to hexagonal SiC with the help of a few additional calculations.

II. METHOD

Our calculation are based on the density functional theory (DFT) in the local density approximation (LDA) for the exchange-correlation functional as parametrized by Perdew and Zunger.[14] We use a plane wave basis code and ultra-soft pseudo potentials[15] provided in the VASP package.[16] As in our previous investigation on SiC defects[17] we use a 211 eV kinetic energy cutoff for the basis set and a very soft C pseudo-potential. This pseudo-potential provides a very good description of important bulk properties of SiC, like heat of formation and lattice parameter (4.312 Å) in good agreement with the experimental value 4.360 Å.[18]

 ©2005 The American Physical Society

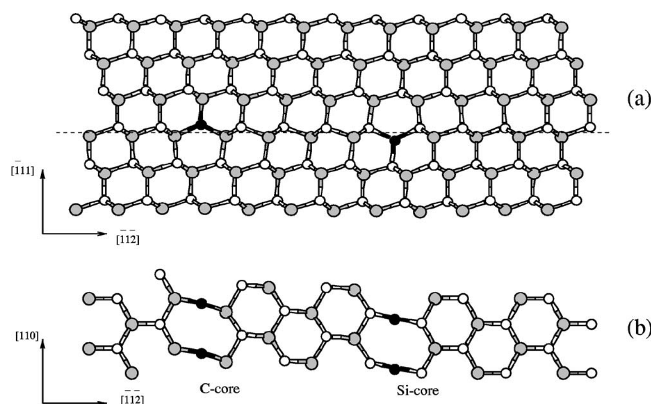

FIG. 1. Atomic configuration containing a dislocation dipole. Dislocations belong to the $\{\bar{1}11\}$ glide planes lying in a $\langle 110\rangle$ direction. The figure shows the configuration sideview on two different planes: (a) a plane normal to the dislocation line; (b) the glide plane where the dislocation belong. The dashed line marks the glide plane shown in (b). White and gray circles represent carbon and silicon atoms, respectively. Black circles represent atoms, belonging to the dislocation core.

We simulate the 30°-partial dislocation using periodic boundary conditions within a supercell approach. The supercell is orthorhombic, with the x, y and z axis parallel to the $\langle 110\rangle$, $\langle\bar{1}11\rangle$, and $\langle\bar{1}1\bar{2}\rangle$ directions of the zinc-blende lattice, respectively. The zinc-blende lattice supercell contains 288 atoms. Edge lengths of the zinc-blende supercells are 6.098, 14.937 and 31.686 Å long. A 30°-partial dislocation dipole was introduced in the supercells. Figure 1 shows, from two different point of view, the atomic structure of the 30°-partial dislocation dipole we used in our calculations. Dislocation dipoles in silicon carbide are formed of two nonequivalent partial dislocations, the so-called Si-core (right side of Fig. 1) and C-core (left side of Fig. 1) partials, differing for the atom type located at the termination of the inserted plane. The cell geometry is such that the dislocations forming the dipole are about 12.0 Å apart along the $\langle\bar{1}1\bar{2}\rangle$ direction. Geometric optimization of the atomic structure was performed by allowing the atoms to relax until the supercell total energy were converged to within 0.01 eV. In the relaxation runs the sampling of the Brillouin zone for the self-consistent calculation of the electronic density was performed using a single k-point ($\|\mathbf{k}\|=0.2575$ Å^{-1}) obtained out of the (112) Monkhorst-Pack mesh.[19] For each equilibrium geometry band structure and band-by-band decomposed electronic densities were computed. For the band structure calculation a string of 21 k-points orthogonal to the [110] plane is used. After the band structure calculation the same set of k-points is used in a self-consistent run to compute the Fermi energy for the supercell. This allowed the evaluation of the Fermi energy for the system under investigation.

III. RESULTS

A. Reconstruction and band structure for the isolated dislocation dipole

Reconstruction patterns and band structure for the 30° partials in SiC have been studied in details by Blumenau *et al.*[13] In this section we compare our results with those of the above mentioned work and point out some features present in the band structure of the unreconstructed dislocation that are essential for understanding the impurity-dislocation system.

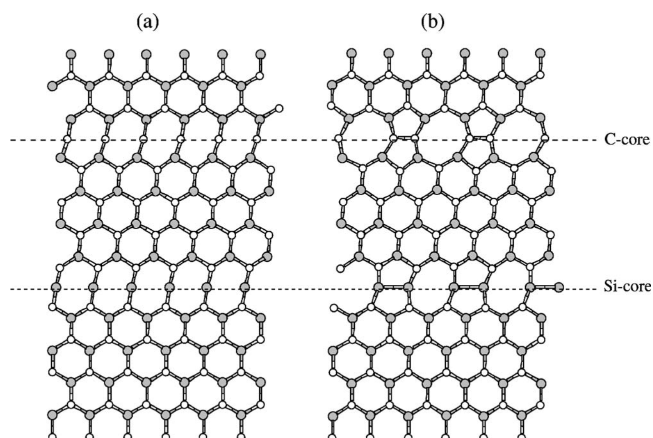

FIG. 2. Atomic configuration of a 30° partial dislocation dipole in the $\{\bar{1}11\}$ glide plane. In the figure, panel (a) shows the unreconstructed C- and Si-core dislocations, while panel (b) shows their fully reconstructed geometries.

In Fig. 2 we show the unreconstructed and reconstructed geometries of the dipole in the $\{\bar{1}11\}$ plane, while in Fig. 3 we compare the band structure along the $\langle 110\rangle$ direction of the bulk system with those of the dislocation dipole for the above mentioned geometries. The charge density plots of the defects levels are reported in Fig. 4. Atoms at the dislocation cores depicted in Fig. 2(a) are threefold coordinated forming with their nearest neighbors a nearly perfect equilateral triangle lying almost parallel to the [110] plane. Because of the low coordination the core atoms show a sp^2 hybridization with a fourth electron occupying a p lone orbital lying along the dislocation line.

The core-core atom distance along the dislocation axis is too large to allow for formation of a chemical bond between core atoms, so that in the *unreconstructed* geometry defect bands crosses the bulk band gap. In Fig. 3(a) the bands marked with circles originate at the C-core partial while those ones marked with squares belong to the Si-core partial. The charge density plots reported in Figs. 4(a) and 4(b) show that defects bands clearly belong to a single dislocation and do not overlap so that each band can be correctly assign to a given partial dislocation. It is worth noticing that each partial dislocation band system depicted in Fig. 3(a) has a band made of two branches, the upper one (marked with open symbols) has a leading *anti-bonding* character while the lower one (marked with filled symbols) is of *bonding* character. As we will see in Sec. IV those branches play an important role in the understanding of the behavior of the impurity-dislocation system.

The dislocation geometry shown in Fig. 2(a) is unstable and undergoes a Jahn-Teller type of symmetry lowering distortion in the form of reconstruction. Reconstruction doubles the periodicity of the dislocation along the $\langle 110\rangle$ direction and splits the defects bonding and an anti-bonding branches,

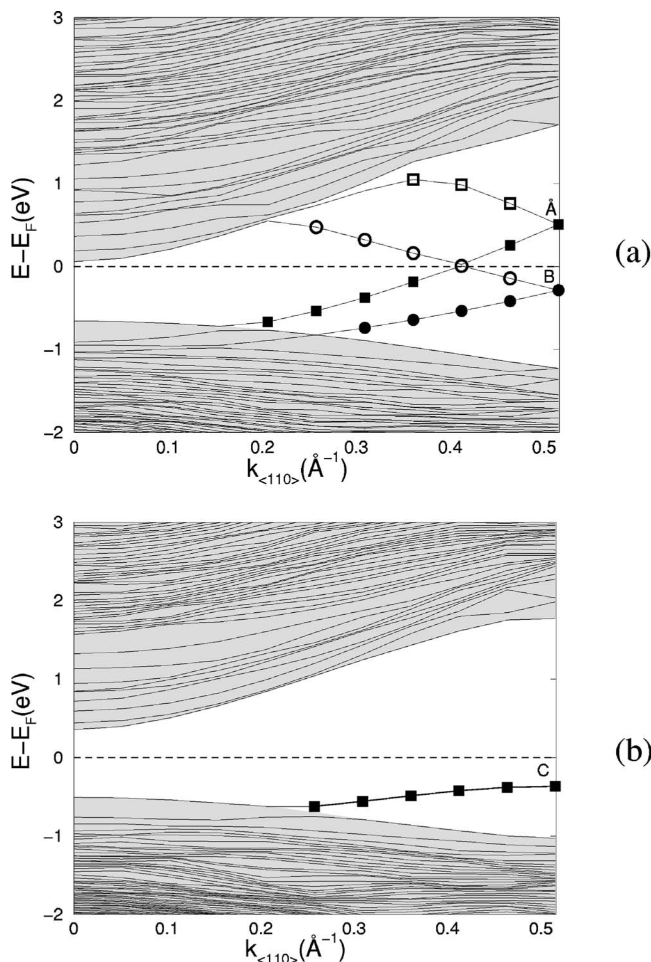

FIG. 3. Band structure along the ⟨110⟩ direction for the 30°-partial dislocation dipole. Panel (a) shows the band structure in the unreconstructed and (b) in the fully reconstructed geometry, respectively. The shaded area represents a background of SiC bulk bands. The circles and squares mark states belonging to the C- and Si-core partial dislocation, respectively. Open symbols highlight the *anti-bonding* branch of the defect band, while filled symbols are used for the *bonding* branch. The dashed line represents the Fermi energy position. Charge density plots at the zone boundaries marked with A, B, and C are shown in Fig. 4.

opening a gap in the defect band structure. In Fig. 3(b) we plot the bands for the reconstructed dislocation whose geometry is shown in Fig. 2(b). Both partials follow the same pattern of reconstruction. Pairs of silicon (carbon) atoms get closer and form dimers along the dislocation axis. In the Si-core partial dislocation distance between the core atoms is reduced from 3.05 to 2.37 Å with a sizable gain of energy: 0.82 eV/pair of core atoms. We remark that the Si—Si distance in the reconstructed core corresponds to the nearest neighbor distance in crystalline silicon. Figure 4(c) shows clearly that a strong covalent bond is formed at the center of the silicon dimer with a concurrent contribution from neighboring carbon atoms. A larger reconstruction characterizes C-core partials where carbons get closer at a distance of 1.68 Å, 9% longer than in diamond, with a gain of energy of 0.58 eV/pair of core atoms. Core atoms distance is nearly halved and a strong bond distortion characterizes a C-core

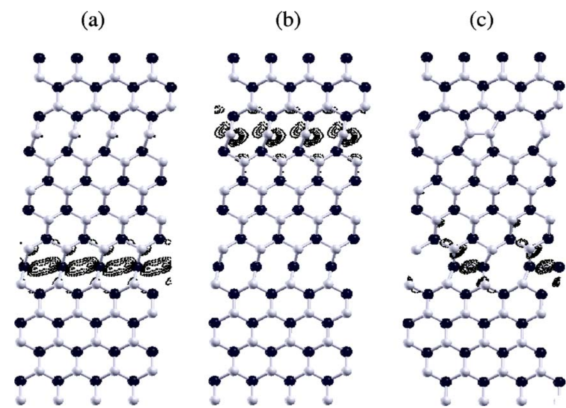

FIG. 4. (Color online) The electronic charge of the gap states on the $\{\bar{1}11\}$ glide plane (as shown in Fig. 2). Panels (a) and (b) refer to the unreconstructed geometry shown in background, while panel (c) refers to the reconstructed dislocation. The states shown in panels (a), (b), and (c) are located at the BZ border of Figs. 3(a) and 3(b), marked with letters A, B, and C, respectively. No localized gap states belong to the C-core reconstructed dislocation.

dislocation. Further approach of the carbon atoms is not energetically favored because it would imply a stretching of the bonds with the neighboring silicons. Indeed in the reconstructed geometry the average bond length to the first silicon neighbors has recovered the bulk value in SiC.

Figure 3(b) shows that reconstruction pushes the defect bands outside the bulk band gap, with the only exception of a narrow band (marked with squares), localized on the Si-core partial dislocation. This band is the bonding branch of the band marked with squares depicted in Fig. 3(a) whose anti-bonding branch lies high in the conduction band. The different behavior between the two partials can be easily understood considering that the hopping term for the C—C covalent bond at the dislocation core is large enough to move outside the gap both branches of the dislocation band regardless their energy in the unreconstructed geometry. At the Si-partial the strength of the covalent bond between core atoms is smaller and the position of the band in the unreconstructed structure is high in the band gap. Therefore a modest branch splitting will push out of the gap only the anti-bonding branch. We conclude that a system formed by an isolated C-core partial in an otherwise perfect SiC crystal, the bulk band gap is free of defect states, while in the case of a Si-core partial the system gap is slightly narrowed by the presence of a band in the lower part of the bulk gap. Our results are in agreement with those obtained by Blumenau *et al.*,[13] where it was found that both dislocations reconstructs. According to the values reported in their work the C—C distance in the C-partial is about 1.80 Å a bit larger than our value of 1.68 Å,[20] while our results for the band structure dispersion along the dislocation axis are in very good agreement with those reported in Ref. 13.

B. Dislocation core charging

In this section we discuss the possible existence of charge *accumulation* at dislocation cores. Charging is an important

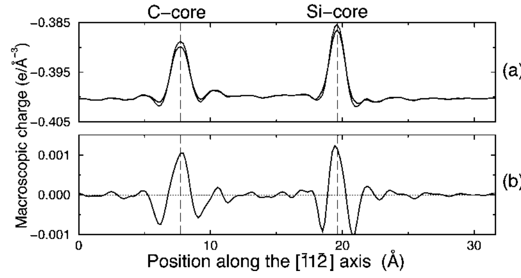

FIG. 5. Macroscopic average of the charge density along the $\langle\bar{1}1\bar{2}\rangle$ direction. Panel (a): Macroscopic average of the actual charge density (thick line) and of a reference system made of superimposed atomic charges (thin line). Panel (b): Differences between the macroscopic averages shown in panel (a).

feature of dislocations: indeed charged dislocations can act as free carriers scatterers as it was found in the case of Ge and GaN.[21,22] Here we want to show that in SiC a straight partial dislocation, in an otherwise perfect crystal, is almost neutral, that is charge transfer between the core and its environment is absent. A rigorous definition of the net charge related to a defect is as problematic as the determination of the ionicity of a polar compound[23] or to the accumulation of charge at the interface between piezoelectric materials.[24] In systems such as semiconductor interfaces this goal is achieved by the macroscopic average[25] of the electronic charge density since the translational invariance of the bulk reference system allows the charge perturbation to be disentangled from the background of bulk-like oscillations. Here we will not address the problem in general, rather we will show, using the macroscopic average technique,[25] that the electronic density distribution around the dislocation core is incompatible with any sizable charge accumulation.

In Fig. 5(a) we show (thick solid line) the macroscopic average of the electronic charge density $\bar{\bar{\rho}}_{\mathrm{SCF}}(z)$ given by

$$\bar{\bar{\rho}}_{\mathrm{SCF}}(z) = \frac{1}{L_x L_y w}\int_0^{L_x}\int_0^{L_y}\int_{z-w/2}^{z+w/2} \rho_{\mathrm{SCF}}(x,y,s)dx\,dy\,ds, \quad (1)$$

where $\rho_{\mathrm{SCF}}(x,y,s)$ is the self consistent electronic charge distribution, L_x, L_y are the supercell edges lengths and w is the running average window width chosen to be equal to $L_z/12$, the period of the bulklike component of the charge density along the $\langle\bar{1}1\bar{2}\rangle$ direction. We see that the macroscopic average has two peaks centered at the dislocation cores surrounded by damped oscillations that extend into the bulklike region between the cores. To show that this does not imply a real charge transfer from the environment to the dislocation core, we draw (thin solid line) the macroscopic average of a reference system that by definition does not have any charge transfer. This reference system is obtained as a superimposition of atomic charge distributions ρ_{ref} defined as

$$\rho_{\mathrm{ref}}(\mathbf{r}) = \sum_{i,t} \rho_{i,t}^{at}(\mathbf{r} - \mathbf{r}_{i,t}), \quad (2)$$

where ρ_t^{at} is the free neutral atom charge for the tth atomic species and $\mathbf{r}_{i,t}$ the position of the ith atom of the tth species. Its macroscopic average $\bar{\bar{\rho}}_{\mathrm{ref}}(z)$ then given by

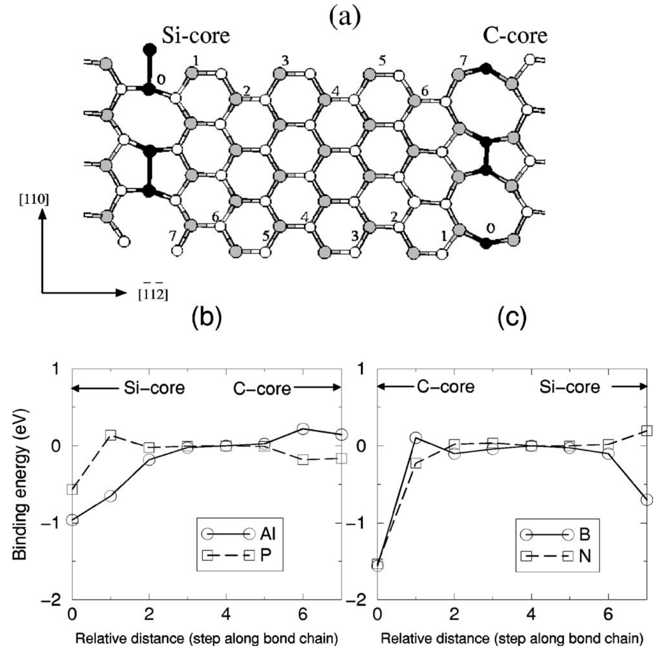

FIG. 6. Energy landscape for single impurities interacting with the dislocation dipole. Panel (a) shows the dislocation dipole in the $\{\bar{1}11\}$ glide plane. The substitutional sites for the Al(B) and P(N) are shown in the upper (lower) side of the figure marked with numbers from 0 to 7. Panel (b) reports the energy for Al and P substituting silicon, and panel (c) for B and N substituting carbon.

$$\bar{\bar{\rho}}_{\mathrm{ref}}(z) = \frac{1}{L_x L_y w}\int_0^{L_x}\int_0^{L_y}\int_{z-w/2}^{z+w/2} \rho_{\mathrm{ref}}(x,y,s)dx\,dy\,ds \quad (3)$$

is plotted in Fig. 5(a) (thin solid line). We see clearly that macroscopic averages in Fig. 5(a) are almost identical. Notably the same peaks at the core positions and the oscillations in the bulklike region are present in both macroscopic charges. In Fig. 5(b) we plot the difference $\bar{\bar{\rho}}_{\mathrm{SCF}}(z)-\bar{\bar{\rho}}_{\mathrm{ref}}(z)$. The diagram does not show any major charge accumulation or depletion around the dislocation cores. The largest deviations from neutrality are very tiny and the small oscillations around the cores indicate local charge redistribution (mostly induced by reconstruction related rebonding) without long range charge transfer between the two partial cores or from the bulk-like environment to the dislocations. Therefore we can state that straight 30° partial dislocations are almost neutral systems. This finding is in agreement with the dislocation band structure that does not reveal the presence of partially filled band (fingerprint of dangling bonds) in the reconstructed dislocations.

C. Dislocation interaction with acceptor and donor impurities

Interaction with impurities is known to affect the mobility and the electrical properties of dislocations.[26] To study the pattern of interaction between the 30-partial dislocations and the most commonly used heterovalent impurities we placed in our defected supercells Al, B, P, and N substitutional impurities at various distance from the dislocations forming the dipole [see Fig. 6(a)]. We employed Al and P to investigate

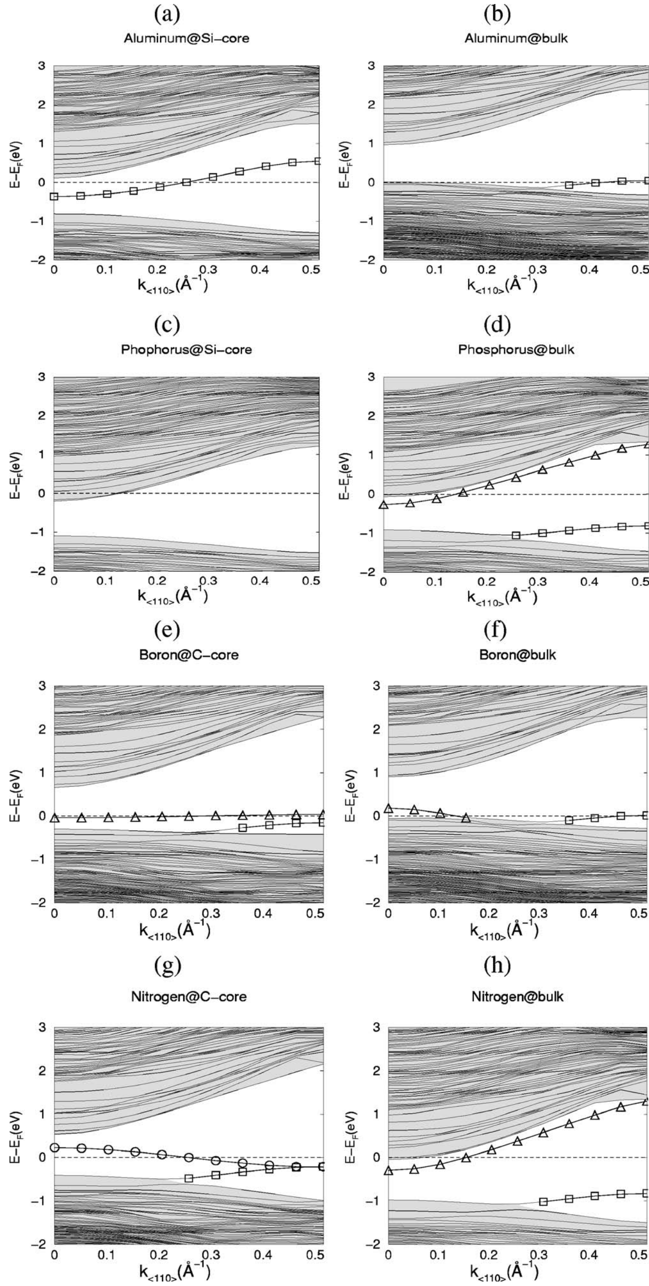

FIG. 7. Band structure along the ⟨110⟩ direction for the 30° partial dislocation dipole in $3C$-SiC with an impurity segregated at the dislocation core, (left panels), and same system with the impurity substituting far from the dislocation core (right panels). Panel (a) Al at the Si-partial core, (b) substitutional Al in a bulklike environment, (c) P at the Si-partial core, (d) substitutional P in a bulklike environment, (e) B at the C-partial core, (f) substitutional B in a bulklike environment, (g) N at the C-partial core, and (h) substitutional N in a bulklike environment. The dashed line represents the Fermi energy position.

the interaction of dislocations with impurities placed at the Si sublattice sites, while B and N were used to investigate those ones substituting at the C sublattice sites. In each configuration the structure of the supercell was fully optimized and the total energy and band structure was calculated as described in Sec. III A. In Fig. 6 we report the relative total energies of the supercell containing the dislocation dipole interacting with the substitutional atom. Since the periodic repeat along the dislocation in the supercell is 6.098 Å, the impurities cannot be considered as totally decoupled defects, therefore, following the strategy of Refs. 7, 8, and 27, we compare the total energy of the supercells where the dopant was substituted at different sites. From Fig. 6 we can extract important information. We see that there exist an energy gain for all of the species of dopants studied to segregate at dislocation cores. In particular Al and P tend to be incorporated at the Si-partial dislocation core [Fig. 6(b)], while B and N are trapped at C-partial dislocation core [Fig. 6(c)]. The segregation energy is larger for the C-partial and nearly independent of the dopant whether it is donor or acceptor. Slightly different is the case of the Si-partial where Al has an higher segregation energy than P. Moreover it looks like that a sizable segregation energy exist for the B toward the Si-partial. Therefore dopant-dislocation interaction and segregation will be an important effect in SiC.

In Fig. 7 we show the band structure along the ⟨110⟩ direction of the dislocation dipole system with a dopant in a substitutional site. Panels on the left show the dopant incorporated at the dislocation core [e.g., Al at the Si-core in panel (a)], panels on the right side show the band structure when the impurity substitutes at a site far from the dislocation cores. As in Fig. 3 we have marked with circles those bands belonging to the C-core partial dislocation and with squares those belonging to the Si-core partial dislocation. It is evident that the position of the impurity with respect to the dislocation core strongly affects the electrical properties of the dopant, indeed the Fermi level of the impurity-dipole systems changes its position as a function of the impurity location. For instance in the case of Al interacting with the Si-core partial dislocation, segregation leads to the formation of an extrinsic band within the bulk band gap and the position of the Fermi levels clearly evidence that the Al impurity is deactivated upon segregation. The same happens for the N impurity segregated at the C-core. On the opposite we find that the P impurity segregated at the Si-core is a donor with a Fermi level even higher that in the case of the impurity in the bulk. In this case segregation looks to enhance the electrical activity of the dopant. Somewhat intermediate is the case of the B at the C-core, in such a case the segregated B gives rise to an extrinsic band but the Fermi level is weakly affected and the B at the C-core come to be a deep acceptor. To help the interpretation of the band structures we have plotted the charge density distributions of the localized defect levels for each of the system studied. Those are reported in Fig. 8 together with the fully relaxed atomic structures. We notice that the incorporation of Al in to the Si-core and N into the C-core leads to dereconstruction of the core structure that on the contrary is kept intact in the case of the P substitutional in the Si-core site and B in the C-core.

IV. DISCUSSION

In this section we provide a rationale to the overall behavior of the impurity-dislocation system.

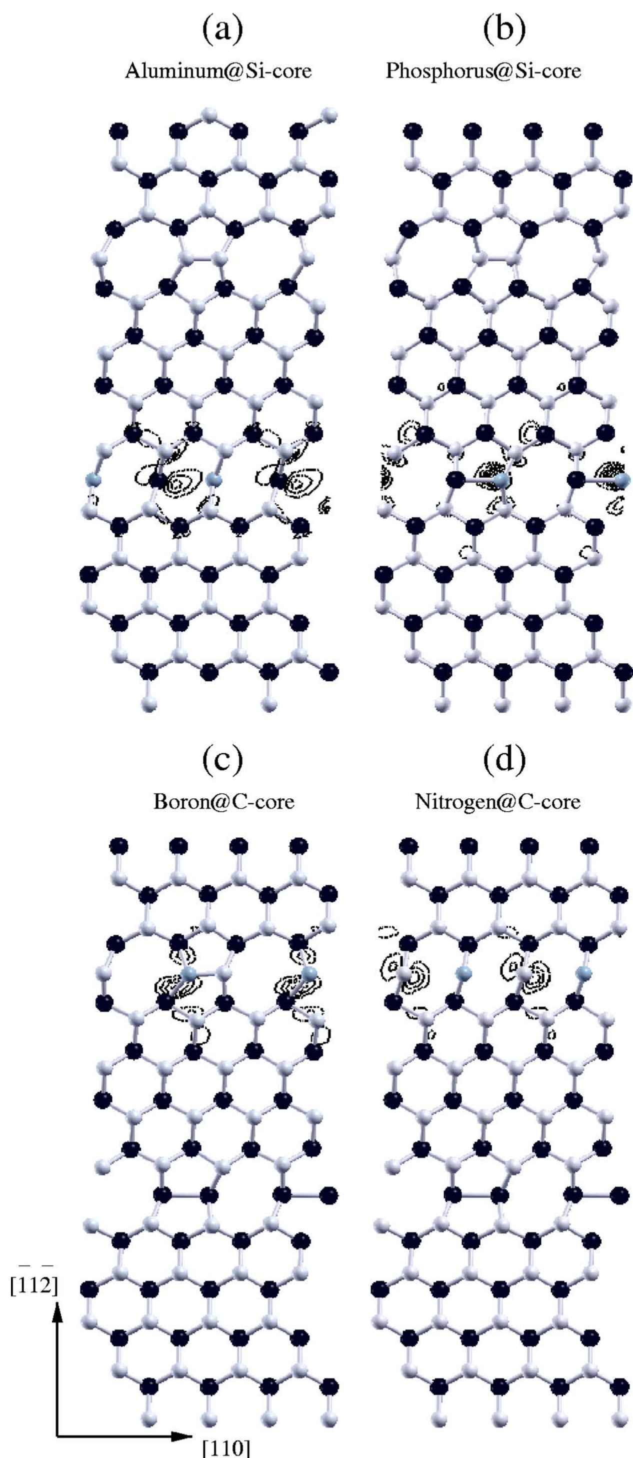

FIG. 8. (Color online) Gap states charge density for a dislocation dipole with an impurity at the core. Panels (a) to (d) refer to Al, P, B, and N impurities.

A. Reconstruction and band structure for the isolated dislocation dipole

Comparing our results with those given in Ref. 28 we find that reconstruction of 30°-partial dislocations in SiC follow the general trend of other semiconductors. The core reconstruction energies per pair of core atoms of cubic semiconductors range from 0.43 to 0.92 eV, with a reconstruction energies ratio $E^{\mathrm{rec}}_{\mathrm{cation\ core}}/E^{\mathrm{rec}}_{\mathrm{anion\ core}}$ from 1.3 to 1.8. In SiC we find a similar ratio of 1.4. Clearly in SiC the difference in the reconstruction energy between Si-core and C-core is due to the additional strain imposed to the C-core structure because of the larger bond distortion. The absence of gap states for the C-core partial dislocation is not unexpected since the covalent bond between C core atoms is very strong and the separation between bonding and antibonding levels will be larger than the bulk gap. The bonding level related to the C—C core bond is a deep resonance in the valence band and the antibonding lies above the conduction band edge. On the contrary in the case of the Si-core partial dislocation, the strength of the covalent Si—Si bond is too weak and not sufficient to push the bonding branch of the extrinsic levels outside the band gap. As a consequence of the imperfect removal of the defects states a narrow band appears at the zone boundary just above the valence band. This *filled* band will not alter the electrical balance of a pure SiC sample but will act as a trap for the holes. Indeed Fig. 7(b), where an Al was placed within the supercell, shows that the Fermi level crosses the small defect band on the right of the figure. This confirms our statement that the presence of a Si-core partial induces a localization of the holes released by the acceptors (e.g., Al) in the neighborhood of the dislocation core, hindering an efficient *p*-doping of SiC.

B. Dislocation interaction with acceptor and donor impurities

Dislocation motion strongly depends on the presence of impurities. Some authors[26] reported experimental data for dislocation mobility in contrast with migration energy calculations for isolated dislocations. It has been suggested that in most materials the mobility of the dislocation is strongly reduced by the pinning effect of segregated impurities. The effect of the impurity on mobility can be deduced from the segregation energy: the higher is the segregation energy, the stronger is the pinning effect on the dislocation. It is known moreover that the effect of pinning is enhanced whenever pairs of impurities are locked at dislocation cores.[7] We find that both acceptor and donor commonly used as dopants in SiC, are responsible for pinning for the 30°-partial dislocations. This result should be only confirmed if impurities dimers are considered. Figure 6 shows clearly that segregation energies for impurities in SiC are comparable or larger than core reconstruction energies. This suggest that mobilities deduced from calculations made on isolated dislocations should be overestimated and applies only to very pure samples.

The impurities with the larger structural effect, among those considered here, are N and Al. We see from Fig. 8(d) that trapping of an N atom at the C core induces a full dereconstruction of the dislocation core. A similar, even if not complete dereconstruction, is induced by the Al at the Si core [see Fig. 8(a)]. This behavior can be rationalized if we consider the effect of the impurities on the dislocation band structure. For instance let us consider the case of Al. Figure 7(b) shows that the band structure of an isolated Al substitutional far from the dislocation core is practically identical to

the band structure of the isolated dislocations shown in Fig. 3(b). The only relevant difference is the position of the Fermi level shifted to the bottom of the band gap in Fig. 7(b). Al segregation completely change this picture. In Fig. 7(a) we see that Al at the Si core gives rise to a very wide extrinsic band lying across the conduction band bottom. We explain the formation of this band as follows. The presence of the acceptor reduces the electrostatic component of the electron binding energy in the dislocation core region affecting the band structure of the reconstructed Si-core dislocation. The bonding branch that in Fig. 7(b) lies in the lower part of the band gap partially overlapping the valence band is shifted upward and now crosses the bulk band gap. Indeed in panel (a) there is no more trace of the defect band on the right side of panel (b). From the band structure in Fig. 7(a), that refers to the case of an ordered array of impurities occupying one site out of two, we can infer the effect of the isolated Al impurity on the dislocation defect electronic structure. The Al—Si bonds that forms at the dislocation core are partially filled and higher in energy with respect to the isolated dislocation defect band and do not act as efficient acceptor levels but are deep acceptor traps. The position of the Fermi energy with respect to the defect band can explain the origin of the dereconstruction. Reconstruction is favored whenever a reduction of the symmetry splits an half filled band into a fully occupied and totally empty one. This is the case of the isolated dislocation. As for the segregated Al impurity, the bonding branch come out to be only partially filled, strongly reducing the driving force for the reconstruction.

The effect of the segregation of P is completely opposite to that of Al. Substitutional P is a good donor, forms a shallow level below the conduction band and shifts the Fermi energy to the bottom of the conduction band, as shown in Fig. 7(d). The net effect of P substitution at Si core is to strengthen the covalent bond among core atoms along the ⟨110⟩ axis. Indeed the P—Si bond length is shorter (2.33 Å), with respect to the Si—Si bond (2.37 Å) and the charge distribution of the states localized at the dislocation core shown in Fig. 8(b) is clearly more localized on the P atom. Because of the larger electronegativity of P with respect to Si and of the preferential localization of the occupied orbitals on the P atoms, in this case the bonding branch of the Si partial is down-shifted in energy and disappears as a resonant state in the valence band. According to the discussion above mentioned in this case reconstruction is favored as is indeed the outcome of the structural calculation [also shown in Fig. 8(b)]. We point out that in the case of segregated P the Fermi level seems to be higher than that for the isolated P and any trace of a shallow donor level disappears in Fig. 7(c). This fact could be a consequence of the coordination of the P at the Si-core site. A substitutional P is normally surrounded by four C atoms, while in this particular case one out of the four neighbors is a Si, that is a less electronegative atom. The hydrogenic donor level associated with the P is now less bound and very likely resonant to the conduction band. Therefore it looks that the effect of segregation on P is to *enhance* its electrical activity as a dopant.

The behavior of the C-core partial dislocation with respect to the impurities is totally opposite to the case of the Si-core partial dislocation. This is not surprising because in this case is the antibonding branch of the states localized at the dislocation core to play a role. The defects states belonging to the C-partial core are more localized on the atoms at the dislocation core. Therefore at variance with the Si-core case here extrinsic bands originate from the covalent bond between the impurities and their neighboring Si partners at the side of the dislocation, as shown in Figs. 8(c) and 8(d). The result of this behavior is the formation of narrow bands localized on the carbons or on the impurities.

Figure 7(f) shows that an isolated B substitutional gives rise to a shallow accepting band (marked with triangles). When incorporated at the C-core dislocation the B does not change significantly the core structure and forms a bond with the neighboring C core atom in the ⟨110⟩ direction and three bonds with the neighboring Si atoms. The level belonging to the B—C bond is far deep in the valence band and is not shown in Fig. 7(e), the B—Si bonds oriented transverse with respect to the dislocation axis form a half-filled dispersionless band (marked with triangles). The net effect is to push up the Fermi level reducing the accepting efficiency of B. We note incidentally that the band marked with squares in Fig. 7(e) belongs to the Si-core dislocation and therefore is absent in a system containing only a C-core dislocation. Therefore in the case of a B segregated at an isolated C core the system will posses only a single half-filled and flat deep accepting band.

As for the N impurity we find that the isolated substitutional shown in Fig. 7(h) is a good donor such as the P. Incorporation into the C core of an N atoms leads to complete dereconstruction of the dislocation core structure. This is somewhat surprising since at a first glance one would expect a strong N—C bonding. Once more a rationale involves the effect of a perturbation on the band structure of the isolated dislocation. Upon segregation N atoms form a deep bonding state with the neighboring Si atoms, this state is a resonance into the valence band [not shown in Fig. 7(g)]. The antibonding branch for the C core lying in the conduction band is pulled down by the presence in the dislocation core of an atom with a large electronegativity. The donation of an electron from N to C fills the anti-bonding branch of the core-core bonds and produces the break up of the N—C bond. It is worth to note that in the case of the anti-bonding branch the defect state shown in Fig. 7(d) is more localized on the C atoms (the less electronegative) while in the case of the bonding defects state in Fig. 7(b) the localization is on the more electronegative P. Because of the extra electron donated by the N atom the upper branch of the C core is half filled and pins the Fermi level midgap. While the dereconstruction of the Si core due to Al segregation is related to the depletion of charge in the bonding branch, here is the donation to the antibonding branch to induce dereconstruction.

V. DISLOCATIONS IN HEXAGONAL SILICON CARBIDE

As mentioned in the Introduction, on the base of simple reasoning, we do not expect a strong dependence of the behavior of a dislocation-impurity system on the kind of polytype structure for the bulk material. In this sections we dis-

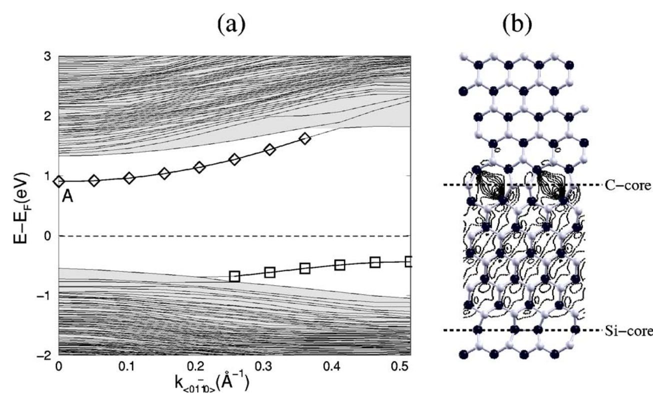

FIG. 9. (Color online) Electronic structure of a reconstructed 30°-partial dislocation dipole in 4H-SiC. Panel (a): Band structure along the $\langle 01\bar{1}0\rangle$ direction. The shaded area represents a background of SiC bulk bands. The diamonds and squares mark states belonging to the stacking faults ribbon and the Si-core partial dislocation, respectively. The dashed line represents the Fermi energy position. Panel (b): Electronic charge of a gap state on the $\{0001\}$ glide plane. The state shown is located at the BZ center of panel (a) marked with letter A.

cuss more in detail the relevance of the bulk structure on the dislocation properties and the interaction of the dislocation with acceptors and donors, with the help of a few calculations performed in hexagonal SiC. An exhaustive investigation of this subject would require a prohibitive amount of calculations, indeed while in the case of cubic SiC there exist only one stable structure, namely the zinc-blende lattice (3C-SiC), in the case of hexagonal SiC we should consider several polytypes such as wurtzite, 4H and 6H. Moreover in the case of hexagonal polytypes there exist different nonequivalent dislocation geometries depending on the choice of the dislocation glide plane with respect to the stacking sequence of the hexagonal lattice.[13] Considering that the most promising hexagonal polytypes for technological applications are 4H and 6H and that we have to restrict the size of our supercell to a tractable dimension, we focused on 4H-SiC.

The supercell used for the 4H polytype contains 384 atoms, it has an orthorhombic shape with the x, y, and z axis parallel to the $\langle 01\bar{1}0\rangle$, $\langle 0001\rangle$ and $\langle\bar{2}110\rangle$ directions of the hexagonal lattice and edge lengths of 6.098, 19.916, and 31.686 Å, respectively. The Si- and C-core partial dislocations axis are oriented in the $\langle 01\bar{1}0\rangle$ directions, with the dislocation dipole lying in the $[0001]$ plane. Our calculations show that Si- and C-core partials in hexagonal SiC have the same patterns of reconstruction found in cubic SiC. We find only a very small difference in the bond lengths between core atoms that in the case of 4H-SiC are slightly shorter, 2.36 Å and 1.66 Å for the Si—Si and C—C pairs, respectively. This is in agreement with the findings of Ref. 13, where the authors do not find relevant differences in the structure and energetics of dislocation between cubic and hexagonal SiC. While differences in the structural details of the dislocations are negligible, band structure calculations show for the reconstructed dislocation in 4H-SiC the existence of a localized state in the gap of the bulk bands not

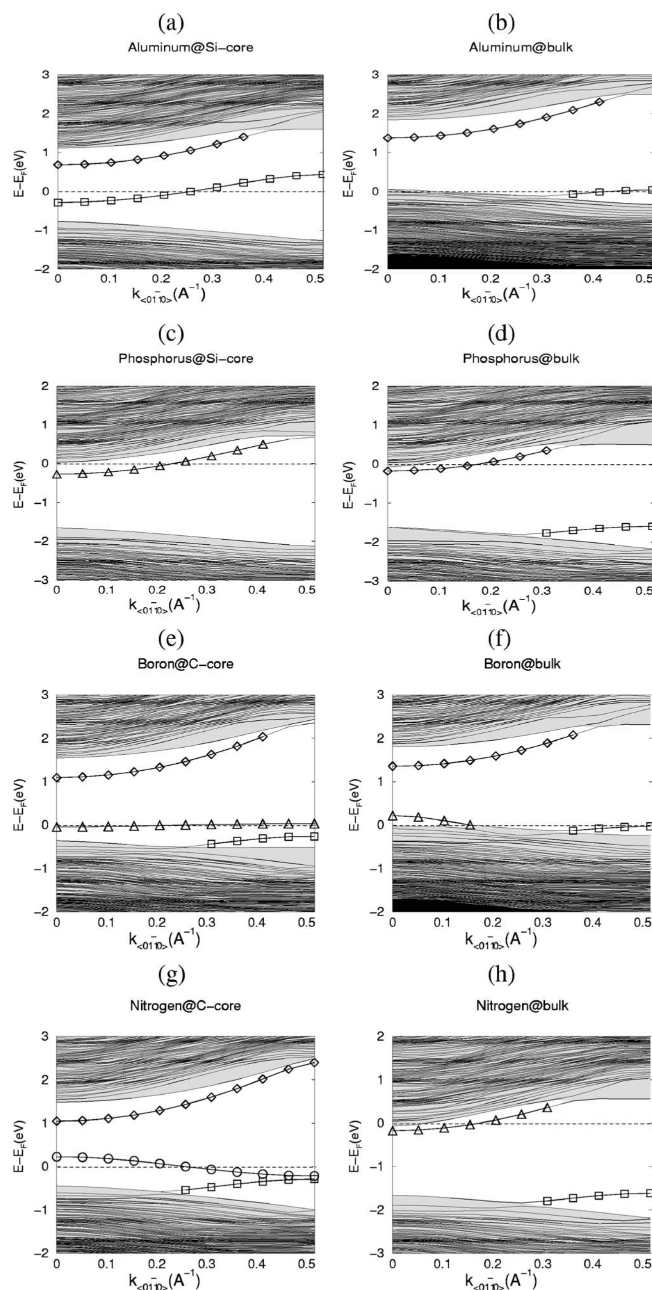

FIG. 10. Band structure along the $\langle 01\bar{1}0\rangle$ direction for the 30° partial dislocation dipole in 4H-SiC with an impurity segregated at the dislocation core (left panels), and same system with the impurity substituting far from the dislocation core (right panels). The localized state depicted in Fig. 9 is marked with diamonds.

present in 3C-SiC. In Fig. 9 we plot the dislocation band dispersion along the $\langle 01\bar{1}0\rangle$ and the charge density of the above mentioned extrinsic band (marked with circles). We see that the state found below the conduction band spread over the whole region delimited by Si- and C-core partials. This is the inner region of the dislocation dipole where a ribbon of stacking faults connects the two partials [Fig. 9(b)]. The electron density is localized mainly around the silicon atoms and behaves in a different way around the two partials cores. It gets inside the C core forming a bond across the

open space of the dislocation that connects the silicon atoms abutting on the dislocation cores. It is repelled by the Si core, clearly because of the different position of the silicon atoms with respect to the core open space. The existence of this extrinsic state is not unexpected, indeed in Refs. 29 and 30 it is shown that stacking faults in hexagonal SiC (but not in the cubic phase) give rise to two-dimensional Bloch states localized around the fault plane. As a consequence of the presence of this state the efficiency of n doping in hexagonal SiC is reduced with respect to the cubic phase.

As for the dislocation interacting with the impurity we find for the dopant segregated at the dislocation core the same geometries discussed in Sec. IV B, confirming that dislocation reconstruction/dereconstruction patterns do not depend on the bulk atomic arrangement. In Fig. 10 we plot the band structure computed for the impurity-dislocation system with the impurity far from the dislocation and segregated at the core. We notice that for the acceptors the similarity of the band structure with those of the cubic phase is striking. The larger gap and the presence of the gap state related to the stacking faults does not influence the electrical properties in the case of p-doped material. Al and B at the dislocation core induce the same effects on the band structure discussed in Secs. IV. Therefore regardless the specific features of the hexagonal polytype band structure acceptors at dislocations cores are electrically deactivated. As for the donors we see that in the case of N segregated at the C-partial core, the band structure in the lower part of the band gap has the same dispersion shown in Fig. 7(g). Given that the Fermi level lies in the lower half of the bulk band gap, the existence of an additional band near the conduction band will not affect the electrical properties of the N at the dislocation core. As in the case of 3*C*-SiC, N is deactivated upon segregation.

We predicted for cubic SiC that P would be the only dopant not deactivated after incorporation at the dislocation core. Here the situation is different for two reasons: (a) n-type material suffers for the trapping of the carriers at the stacking fault originating at the dislocation core, (b) our calculation for P at the Si-partial core shows that the donor level of P is not resonant to the conduction band as in the case of 3*C*-SiC. The latter is very likely a consequence of the larger gap width in 4*H*-SiC. Those findings suggest that in the hexagonal phase n-doping by P could not be so effective as in cubic SiC, nevertheless we find P the only dopants (among the studied) that is not completely deactivated in SiC. Those results indicate that the behavior of a dislocation toward acceptor dopants is by and large independent of the bulk phase, while for the donor it looks like less favorable in the hexagonal phase because of the presence of localized states in the upper side of the bulk band gap.

VI. CONCLUSIONS

In this work we have investigated the properties of the 30°-partial dislocations in SiC. Our results for the isolated dislocation dipole fairly agree with previous investigations.[13] The calculations for the impurity-dislocation system show that there is a strong tendency for the impurities to segregate at the dislocation core. This result supports the hypothesis that dislocation motion is strongly affected by impurity pinning effects. Moreover segregation changes the electrical properties of the dopants. When trapped at the Si-partial dislocation core, an acceptor such as Al is inactivated and forms a deep state in the band gap. A donor such as a P, trapped at the same dislocation core, is still active as donating impurity. In the case of the C-core partial dislocation, segregation strongly affects both acceptors and donors electrical properties. B is transformed into a deep acceptor while N, besides full dereconstruction of the dislocation core, leads to the formation of an extrinsic band located at midgap, pinning the Fermi level. We discussed our results in terms of a simple model that should be easily generalized to other semiconductors. Finally we considered the possible effects of the bulk structure (cubic versus hexagonal phase) on the dislocation and its interaction with doping impurities. We find that the presence of dislocations makes hexagonal SiC less suitable for n-type doping, because of the existence of a gap state related to the stacking fault originating at the dislocation cores.

ACKNOWLEDGMENTS

This work has been funded by MIUR under project FIST-2001 “PROMOMAT.” We acknowledge computational support by INFM under “Parallel Computing” Initiative. Charge density plots have been produced using XCRYSDEN.[31]

*Author to whom correspondence should be addressed. Email address: fabio.bernardini@dsf.unica.it

[1] Y. M. Tairov and V. F. Tsvetkov, J. Cryst. Growth **43**, 209 (1978).
[2] D. L. Barrett, R. G. Seidensticker, W. Gaida, R. H. Hopkins, and W. J. Choyke, J. Cryst. Growth **109**, 17 (1991).
[3] Y. Tajima, K. Kijima, and W. D. Kingery, J. Chem. Phys. **77**, 2492 (1982).
[4] R. F. Davis, G. Kelnerm, M. Skur, J. W. Palmour, and J. A. Edmond, Proc. IEEE **79**, 677 (1991).
[5] P. O. Å. Persson, L. Hultman, M. S. Janson, A. Hallen, and R. Yakimova, J. Appl. Phys. **93**, 9395 (2003); P. O. Å. Persson, L. Hultman, M. S. Janson, A. Hallen, R. Yakimova, D. Panknin, and W. Skorupa, J. Appl. Phys. **92**, 2501 (2002).
[6] H. Alexander, in *Dislocations in Solids*, edited by F. R. N. Nabarro (North-Holland, Amsterdam, 1986), Vol. 7, p. 115.
[7] A. Antonelli, J. F. Justo, and A. Fazzio, J. Appl. Phys. **91**, 5892 (2002).
[8] Theodore Kaplan, Feng Liu, Mark Mostoller, M. F. Chisholm, and V. Milman, Phys. Rev. B **61**, 1674 (2000); Theodore Kaplan, Mark Mostoller, and M. F. Chisholm Phys. Rev. B **58**, 12865 (1998).
[9] M. I. Heggie, S. Jenkins, C. P. Ewels, P. Jemmer, R. Jones, and P. R. Briddon, J. Phys.: Condens. Matter **12**, 10263 (2000).
[10] I. Yonenaga, T. Taishi, X. Huang, and K. Hoshikawa, J. Appl.

Phys. **89**, 5788 (2001).
[11] P. Sitch, R. Jones, S. Öberg, and M. I. Heggie, Phys. Rev. B **50**, 17717 (1994).
[12] I. Yonenaga, T. Taishi, X. Huang, and K. Hoshikawa, J. Appl. Phys. **93**, 265 (2003).
[13] A. T. Blumenau, C. J. Fall, R. Jones, S. Öberg, T. Frauenheim, and P. R. Briddon, Phys. Rev. B **68**, 174108 (2003).
[14] J. P. Perdew and A. Zunger, Phys. Rev. B **23**, 5048 (1981).
[15] D. Vanderbilt, Phys. Rev. B **41**, R7892 (1990).
[16] G. Kresse and J. Hafner, Phys. Rev. B **47**, R558 (1993); G. Kresse, thesis, Technische Universität Wien, 1993; G. Kresse and J. Furthmüller, Comput. Mater. Sci. **6**, 15 (1996); Phys. Rev. B **54**, 11169 (1996).
[17] F. Bernardini, A. Mattoni, and L. Colombo, Eur. Phys. J. B **38**, 437 (2004).
[18] *Landolt-Börnstein: Numerical Data and Functional Relationships in Science and Technology*, edited by O. Madelung, New Series, Group III, Vol. 17a (Springer, Berlin, 1982), p. 49.
[19] H. J. Monkhorst and J. D. Pack, Phys. Rev. B **13**, 5188 (1976).
[20] This small difference can be attributed to the different approximations used in the solution of the self-consistent Kohn-Sham equations, in particular in Ref. 13 a Gaussian basis was used to expand the wave functions, while in our case a plane-wave approach was used. In spite the different methodological approach the overall picture we get is the same of Ref. 13.
[21] W. T. Reed, Philos. Mag. **45**, 775 (1954).
[22] H. M. Ng, D. Doppalapudi, T. D. Moustakas, N. G. Weimann, and L. F. Eastman, Appl. Phys. Lett. **73**, 821 (1998).
[23] A. García and M. L. Cohen, Phys. Rev. B **47**, 4215 (1993); A. García and M. L. Cohen, Phys. Rev. B **47**, 4221 (1993).
[24] F. Bernardini and V. Fiorentini, Phys. Rev. B **57**, R9427 (1998).
[25] A. Baldereschi, S. Baroni, and R. Resta, Phys. Rev. Lett. **61**, 734 (1988).
[26] P. Pirouz and J. W. Yang, Ultramicroscopy **51**, 189 (1993); X. J. Ning, and P. Pirouz, Inst. Phys. Conf. Ser. **142**, 449 (1996).
[27] A. Maiti, T. Kaplan, M. Mostoller, M. F. Chisholm, S. J. Pennycook, and S. T. Pantelides, Appl. Phys. Lett. **70**, 336 (1997).
[28] J. F. Justo, A. Fazzio, and A. Antonelli, J. Phys.: Condens. Matter **12**, 10039 (2000).
[29] Hisaomi Iwata, Ulf Lindefelt, Sven Öberg, and Patrick R. Briddon, Phys. Rev. B **65**, 033203 (2002).
[30] M. S. Miao, Sukit Limpijumnong, and Walter R.L. Lambrecht Appl. Phys. Lett. **79**, 4360 (2001).
[31] A. Kokalj, J. Mol. Graphics Modell. **17**, 176 (1999). Code available from http://www.xcrysden.org/.